ADVANCED MATERIALS INTERFACES
www.advmatinterfaces.de

Large-Range, Reversible Directional Spreading of Droplet on a Double-Gradient Wrinkled Surface Adjusted Under Mechanical Strain

*Hao Chai, Ye Tian, Sihang Yu, Binbin Cao, Xiang Peng, Zheng Zhang, Aiping Liu, and Huaping Wu**

Dynamical regulation to unidirectional wetting has received considerable attention in recent years due to its important role in flexible electronics, microfluidics, drug transportation, and so forth. It is of great significance to prepare a surface which allows the droplet to spread directionally on it with the length of droplet reversibly fluctuated within a broad range under external stimulation. In this paper, a double-gradient wrinkled structure is prepared by constructing the structure-gradient pillar arrays on a mechanics-adjusted wrinkled surface and subsequently making chemical gradient by oxygen plasma treatment. Under the synergistic effect of the structural gradient, chemical gradient, and wrinkled structure, the droplet can undergo unidirectional spreading and realize dynamic regulation of the spreading length on the flexible structure. This will provide a propagable method for the regulation of surface wetting.

1. Introduction

The effective controlling for the surface wettability has evoked significant interest due to its potential applications in microfluidics,[1–3] self-cleaning,[4,5] filtration,[6] lab-on-a-chip devices,[7–9] and oil-water separation.[10] The wettability of a surface is usually regulated by applying external stimuli such as light,[11,12] heat,[13,14] photothermy,[15] electricity,[16–19] magnet,[20,21] mechanical strain,[22,23] and acoustic waves.[24] Among these stimuli, the mechanical strain introduction is relatively simple and environmentally friendly, and therefore frequently used to tune surface wettability.[25–27] Additionally, the surface chemical composition and geometric morphology can also affect surface wettability.[28–36] By adjusting the surfaces with wettable gradients (such as structural gradients and chemical gradients),[37–39] asymmetric structures[40–44] or bioinspired structures,[45–51] a droplet spreading on these surfaces can be well manipulated. However, singly structural or chemical gradient surfaces can just carry out the conversion of surface wetting properties between hydrophobic and hydrophilic (or between hydrophobic and super-hydrophilic) but not favor the droplet to spread or move over a long distance due to the influence of the intrinsic contact angle.[52,53] Therefore, a combination of structural and chemical gradients is usually applied to better modulate the conversion of surface wetting property from super-hydrophobic to hydrophilic. For instance, the Yang's group infiltrated a silicon template with a morphology gradient into a trichlorosilane solution, forming a wettable gradient surface which could be converted from super-hydrophobic to hydrophilic.[54] Han et al. placed a polystyrene sheet with a gradient array into a temperature gradient field and an acidic gradient environment in two orthogonal directions, obtaining a two-dimensional composite wetting gradient surface which could change from super-hydrophobic to hydrophilic.[55] These researches indicate that a composite gradient can result in a bigger change in surface wettability than a single wettable gradient. Additionally, the Zheng's group combined a chemical gradient and Laplace pressure gradient via a special wedge-pattern to form an asymmetric structure, achieving the spontaneous and pumpless directional motion of micro-sized droplet on a highly adhesive surface.[40] Wang et al. used direct laser writing to create tree-shaped hierarchical cones on a super-hydrophobic TiO_2 film with a surface energy gradient and Laplace pressure gradient,[42] thereby precisely and continually driving tiny water droplet spreading. According to the continuous and directional water transport on the peristome surface of *Nepenthes alata*,[47] the Chen's group proposed a bionic structure design and realized a biologically inspired continuous unidirectional liquid spreading.[45] However, once the biomimetic structure was completed, it was difficult to precisely regulate the spreading length of the droplet via external stimuli.

H. Chai
Zhijiang College of Zhejiang University of Technology
Shaoxing 312030, China
Y. Tian, S. H. Yu, B. B. Cao, Dr. X. Peng, Prof. Z. Zhang, Prof. H. P. Wu
Key Laboratory of E&M
Ministry of Education & Zhejiang Province
Zhejiang University of Technology
Hangzhou 310014, China
E-mail: wuhuaping@gmail.com, hpwu@zjut.edu.cn
Prof. A. P. Liu
Center for Optoelectronics Materials and Devices
Key Laboratory of Optical Field Manipulation of Zhejiang Province
Zhejiang Sci-Tech University
Hangzhou 310018, China
The ORCID identification number(s) for the author(s) of this article can be found under https://doi.org/10.1002/admi.201901980.

DOI: 10.1002/admi.201901980

Anisotropic wetting involves the inhomogeneous distribution of liquid and accompanying wetting properties upon a surface.[56,57] Anisotropic wetting phenomena include both dynamic properties (e.g., different sliding angles in different directions[58–60]) and static properties (different static contact angles in different directions[61–63]). Among the structures used to study the wettability of anisotropic surface, wrinkled structures are the most common.[64–66] Previous works have studied the wettability of wrinkled surfaces from both theoretical[67,68] and experimental[69–72] perspectives. For the rigid wrinkled surface, once the surface is prepared, its wettability is difficult to change. The soft wrinkled structure with anisotropy and stretching reversibility is confirmed to be a good choice for the mechanical regulation of wettability.[73–78] Rhee et al. applied the stress to the surface of soft materials to switch the orientation of the wrinkle, thereby changing the direction of the liquid flow.[79] Inspired by this, Kwon et al. proposed a simply responsive mechanical system on patterned soft surfaces to manipulate both the anisotropy and orientation of liquid wetting.[80] However, they did not study the spreading length of the droplets on this soft material system and corresponding control method.

In this work, we present a double-gradient wrinkled structure (structural gradient and chemical gradient) on a soft material. Specifically, we first select appropriate parameters of gradient pillar arrays and chemical gradients to achieve the transition of surface wettability from hydrophobic to super-hydrophilic and the droplets are able to undergo unidirectional spreading on this surface. Next, we select PDMS (polydimethylsiloxane) film and VHB (very high bonding) tapes as the upper and lower layers of the structure and study the effect of different strains on the spreading length of the droplets. Finally, in situ and ex situ control of anisotropic droplet spreading are achieved by mechanical regulation of the flexibly structured surface in a controlled fashion, which would have potential engineering applications in microfluidic valves, micro- and nanofabrication of complex structures, and cell transport manipulation.

2. Results and Discussion

2.1. Surface Characterization of Double-Gradient Wrinkled Structure

The double-gradient wrinkled structure was prepared by spin-coating PDMS film on the commercial silicon template with gradient hole arrays, transferring it to the pre-stretched VHB tapes surface, releasing the pre-stretched VHB tapes and finally space-limited oxygen plasma treating to the surface (see details in Section 4 and Figure S1, Supporting information). **Figure 1**

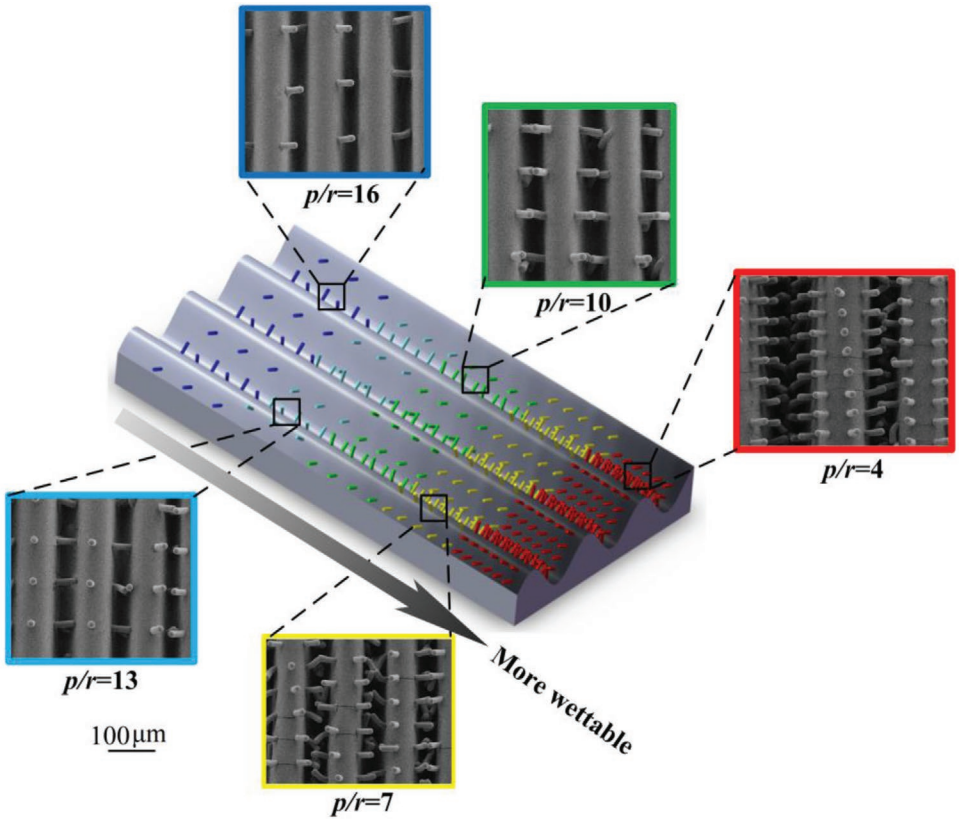

Figure 1. A schematic diagram and scanning electron micrographs of the double-gradient wrinkled structure. p is the center distance between two adjacent pillars ($p = 20$, 35, 50, 65, and 80 μm). r is the radius of pillars ($r = 5$ μm). The different gradients are shown with different colors (indigo, azure, green, yellow, and red). The $\Delta p/r$ is 3, and the amount of pre-strain is 200%. The scale bar is 100 μm. The surface wettability is gradient transitional after plasma treatment, as schematically shown from light gray, gray to dark gray toward more hydrophilic area. The height of the pillars is 40 ± 2 μm.

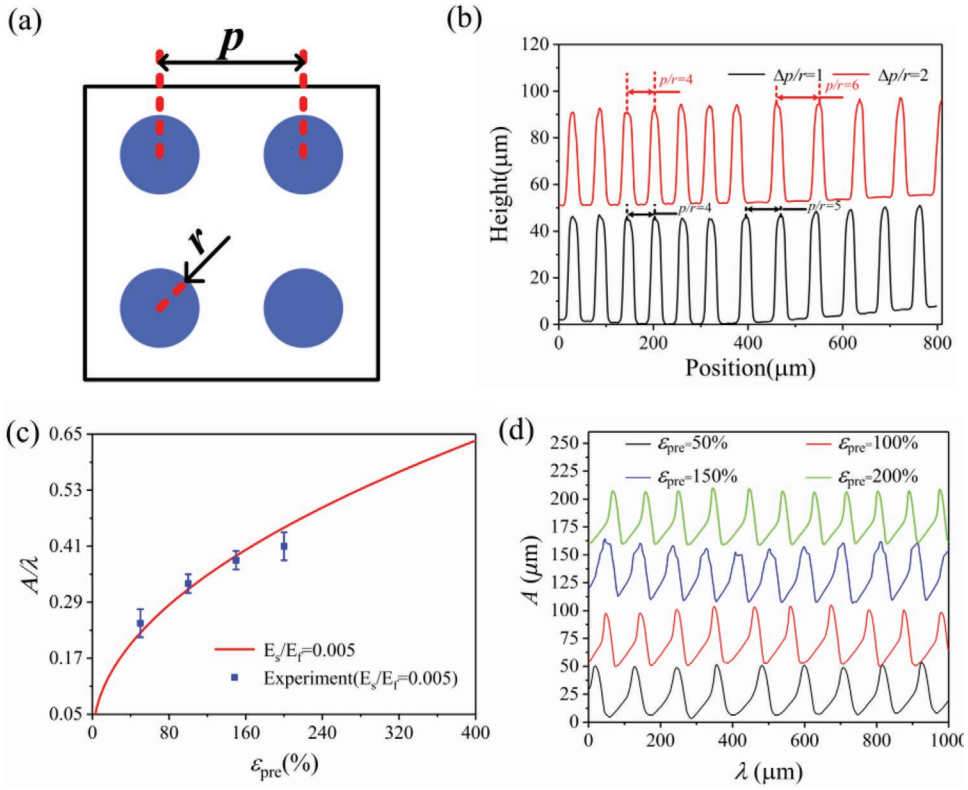

Figure 2. a) Schematic diagram of pillar arrays; the blue pattern represents the pillar, r is the radius of the pillar, which is constantly equal to 5 μm, and p is the distance between the center of the pillars, which changes with the gradient. b) Numerical results from laser microscope of the pillar arrays with different $\Delta p/r$, the height of the pillars is 40 ± 2 μm. c) The relationship between relative height (A/λ) and pre-strain (ε_{pre}), the red line represents theoretical result and the blue dots represent the experimental results under different ε_{pre} values. d) Numerical results from laser microscope of the wrinkle structure. Four different colored lines represent the wrinkle dimensions formed under four different ε_{pre} values.

shows a schematic diagram and several scanning electron microscope images of the double-gradient wrinkled structure. Here we define the center distance between two adjacent pillars as p, and the radius of pillars as r (**Figure 2**a). Therefore, the ratio of p/r indicates the intensity of the pillars with different gradients, and $\Delta p/r$ represents the variation amplitude in p/r of two adjacent arrays. It can be seen that when r = 5 μm, with the decrease of p from 80 to 20 μm ($\Delta p/r$ = 3), the density of pillars is increasing, as schematically shown with different colors (indigo, azure, green, yellow, and red) for different gradients (Figure 1). After the surface is treated by space-limited oxygen plasma to form a chemical gradient, the surface wettability is gradient transitional, as schematically shown from light gray, gray to dark gray toward more hydrophilic area (which is further confirmed in Section 2.2).

Additionally, we can deliberately design the variation amplitude in p/r of two adjacent arrays. For example, when $\Delta p/r$ = 1, the first pillar arrays are constructed with p/r = 4, followed by the ones with p/r = 5, 6 and so on. While when $\Delta p/r$ = 2, the first pillar arrays are constructed with p/r = 4, followed by the ones with p/r = 6, p/r = 8 and so on. The surface topography of pillar arrays with different pitch gradients ($\Delta p/r$ = 1, 2) are also observed by a laser microscope. A well periodic wrinkled structure is demonstrated in Figure 2b.

According to previous studies, the wrinkle wavelength (λ) and amplitude (A) are given by[67,81–83]

$$\lambda = 2\pi h_f \left(\frac{\bar{E}_f}{3\bar{E}_s}\right)^{1/3} \tag{1}$$

and

$$A = h_f \left(\frac{\varepsilon}{\varepsilon_c} - 1\right)^{1/2} \tag{2}$$

where $\bar{E} = E/(1-\nu^2)$, E, h, ν, and ε are the elastic modulus, film thickness, Poisson's ratio, and applied strain, and subscripts f and s refer to the film and the substrate, respectively. Here the effect of surface microstructure on the thickness of the film is omitted. The critical strain (ε_c) must be applied for wrinkle formation and is given by[84,85]

$$\varepsilon_c = \frac{1}{4}\left(\frac{3\bar{E}_s}{\bar{E}_f}\right)^{2/3} \tag{3}$$

The relationship between the relative height (A/λ) of the wrinkle structure and the pre-strain (ε_{pre}) can therefore be obtained with the following equation

$$\frac{A}{\lambda}=\frac{1}{2\pi}\frac{\left(\frac{\varepsilon_{pre}}{\varepsilon_c}-1\right)^{1/2}}{\left(\frac{\overline{E}_f}{3\overline{E}_s}\right)^{1/3}}=\frac{1}{\pi}\sqrt{\varepsilon_{pre}-\varepsilon_c} \quad (4)$$

It is known that the elastic modulus of PDMS is 4 MPa, and that of VHB tape is 0.02 MPa, which can be substituted into Equation (4) to obtain a theoretical diagram, as shown in Figure 2c. We can see that the relative height (A/λ) increases when ε_{pre} increases. In order to verify the effect of ε_{pre} on the size of wrinkle structure, four wrinkle surfaces with pre-stretching of 50%, 100%, 150%, and 200% were prepared. From the profile results obtained from laser microscope (shown in Figure 2d), we can clearly see that as ε_{pre} increases, the λ of the wrinkle decreases and the A increases. The relative heights of the wrinkle structures at ε_{pre} of 50%, 100%, 150%, and 200% are 0.25 ± 0.03, 0.33 ± 0.02, 0.38 ± 0.02, and 0.41 ± 0.03, respectively. The experimental data are in good agreement with the theoretical ones (Figure 2c).

2.2. Wetting Behavior of Droplets on the Flat Surface with Chemical Gradient and Structural Gradient

Prior to investigating the wetting behavior of droplets on the surface with double-gradient structures, we first consider wetting behavior of droplets on the surface with either chemical gradient or pillar array gradient. Short movement of the droplets on the pillar arrays gradient and weak directional spreading of the droplets on the chemical gradient surface can be obtained (detailed analysis in Parts S2 and S3, Supporting information). Therefore, we combine pillar arrays gradient with chemical gradients in an attempt to achieve longer directional spreading. For a droplet in the wetting gradient surface, the driving force (F_d) can be described as[86–88]

$$F_d=\gamma_{LV}\pi\frac{d\cos\theta}{dx}R^2=-\gamma_{LV}\pi\sin\theta\frac{d\theta}{dx}R^2 \quad (5)$$

where γ_{LV} is the interfacial tension of the solid–liquid interface, and R is the radius of the base of the droplet and θ is the position-dependent contact angle of the liquid droplet. The hysteresis force (F_h), due to CA hysteresis, is always opposite to the moving direction and can be expressed as[87,88]

$$F_h=2R\gamma_{LV}\left(\cos\theta_r-\cos\theta_a\right) \quad (6)$$

where θ_r and θ_a are the receding and advancing contact angles, respectively, when the contact angle is θ. The spreading of the droplets is determined by the F_d and the F_h. When $F_d < F_h$, the droplets do not move; otherwise the droplets begin to move along the wetting gradient direction. Here, we select the most sparse pillar array area as the starting position of the droplet spreading (**Figure 3**a). Figure 3b shows the change in the contact angle θ at different positions of the composite wetting gradient surface treated by oxygen plasma at an inclination angle of the shield θ_T and same pillar arrays ($\Delta p/r = 3$). The wetting gradient surface exhibits a transition from hydrophobic to hydrophilic. It can be seen from Equation (5) and Figure 3b that under the same θ, F_d increases as $\frac{d\theta}{dx}$ increases, while $\frac{d\theta}{dx}$ at $\Delta p/r = 3$ and $\theta_T = 60°$ is the largest among the three composite gradients. So theoretically the droplets can spread longer on the surface of composite gradient at $\Delta p/r = 3$ and $\theta_T = 60°$. This is confirmed by experimental measurement. It can be clearly seen that the droplets can carry out a longer directional spreading on the composite wetting gradient surface ($\Delta p/r = 3$, $\theta_T = 60°$, Figure 3c) when compared with the ones on either pillar arrays gradient surface or chemical gradient surface (Figures S2b and S3b–d, Supporting information). The spreading of droplets on the surface is improved as the parameters of $\Delta p/r$ and θ_T increase (Figure 3d). The maximum length that the droplet spreads on the surface of $\Delta p/r = 3$ and $\theta_T = 60°$ is 4.91 mm. A detailed droplet spreading diagram is shown in Figure S4, Supporting information.

2.3. Effect of Wrinkled Structure to the Wettability of Composite Gradient Surface

In order to further increase the spreading length of a droplet, we introduced a wrinkle structure to add anisotropic properties to the surface. As is well known,[47–52] on the surface of an anisotropic structure, a droplet is more easily spreading along the axial of the anisotropic structure and is constrained in the direction perpendicular to the axial of the anisotropic structure. Same to the composite wetting gradient surface, we select the most sparse pillar array area as the starting position of the droplet spreading. As shown in **Figure 4**a, the droplet on the surface with chemical gradient spreads a little bit due to the existence of gradient force. With the combination of chemical gradient and pillar arrays gradient, the droplet spreads unidirectionally as designed, and the spreading length has been greatly improved (shown in Figure 4b). The introduction of wrinkle structure can further adjust the wettability of the composite gradient surface (Figure 4c), since droplet spreading is constrained in the direction perpendicular to the axial of the wrinkle structure, and the spreading length along the axial of the wrinkle structure is therefore further promoted.

Figure 5 shows the experimental spreading length of the droplets on double-gradient wrinkled surface under different ε_{pre} values. It can be seen that the wrinkle structure results in different degrees of increase in the spreading length of the droplet on the surface. In other words, the size of the wrinkle structure greatly affects the spreading length of a droplet. On a flat surface with pillar arrays gradients and chemical gradients, a droplet of 5 µL can spread up to 4.91 mm ($\Delta p/r = 3$, $\theta_T = 60°$, Figure 3d). When the wrinkle structure is introduced into the surface with composite wetting gradient, the spreading length of the droplet is significantly increased to 10.7 mm when $\Delta p/r = 3$, $\theta_T = 60°$, and $\varepsilon_{pre} = 200\%$ (Figure 5). A detailed droplet spreading diagram and statistical data of spreading length of the droplet are shown in Figures S5–S7 and Figure S8, Supporting information, respectively.

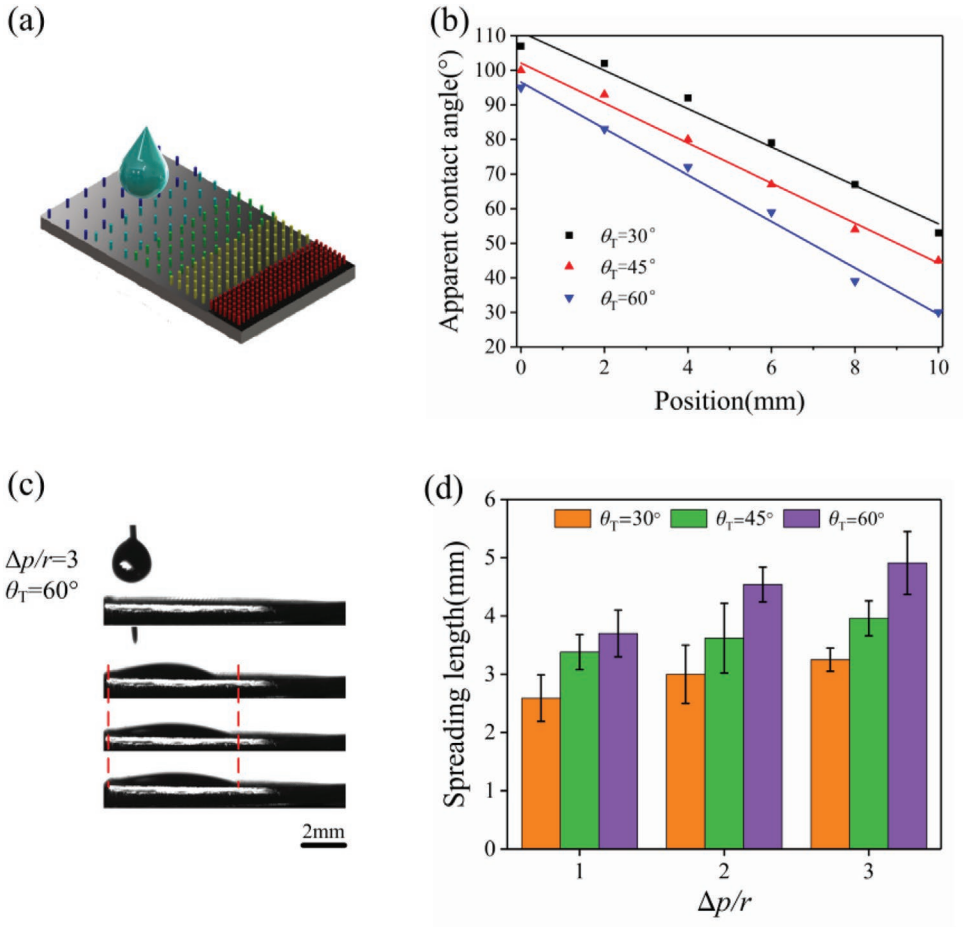

Figure 3. Wetting behavior of droplets on the surface with composite gradients (chemical gradients and pillar arrays gradients). a) The schematic diagram of a droplet dropped on a composite gradient surfaces. b) Apparent contact angles at different positions of the composite wetting gradient structure. The pillar arrays selected are $\Delta p/r = 3$, and three different colored lines represent three different chemical gradients. c) The movement of the droplet on the composite wetting gradient structure with $\Delta p/r = 3$ and $\theta_T = 60°$. Scale bar is 2 mm. d) Experimental data of the spreading length under different parameters.

2.4. Ex Situ Regulation of External Strain and Its Effect to the Spreading Length of Droplets

Since the PDMS upper layer and VHB lower layer are both flexible, the structural size of the flexible wrinkle structure can be intelligently adjusted by applying external strain. Figure 5 shows the effect of the pre-strain on the droplet spreading length. Therefore, we can apply external strain to the already formed wrinkle structure to adjust the size of the wrinkle structure, thereby changing the directional spreading length of the droplet. As schematically shown in **Figure 6**a, we selected the double-gradient wrinkled surface ($\theta_T = 60°$) with $\varepsilon_{pre} = 200\%$ as the experimental object, and stretched it to 100% for the initial position of the experiment, and then the 5 µL droplet was placed onto the surfaces. As shown in Figure S9, Supporting information, the application of compressive strain causes the A/λ of the wrinkle structure to become larger. In other words, the wrinkle structure becomes steep and the spreading length of the droplet increases. As the wrinkle structure gradually becomes gentler after the application of the tensile strain, the influence of the wrinkle structure on the spreading length is reduced and so the spreading length of the droplet reduces. Detailed numerical results of the spreading length are shown in Figure 6b. When a compressive strain of 100% is applied, the droplet spreads to a length of 10.7 mm on the surface, and the spreading length decreases as the compressive strain decreases. When the tensile strain is applied, the spreading length decreases as the tensile strain increases. To further characterize the directional spreading of a droplet, the droplet anisotropy can be defined by using the normalized length ratio as follow:

$$\text{Anisotropy} = \frac{l(\parallel)}{l(\perp)} \tag{7}$$

The changing trend in anisotropy is similar to the one observed for the spreading length. When the tensile strain is applied, the wrinkle structure becomes more subtle, and the anisotropic effect gradually disappears, and conversely, the anisotropic effect increases. When a tensile strain of 100% is applied, the anisotropy index approaches 1 (Figure 6c), indicating that the droplet becomes more circular.

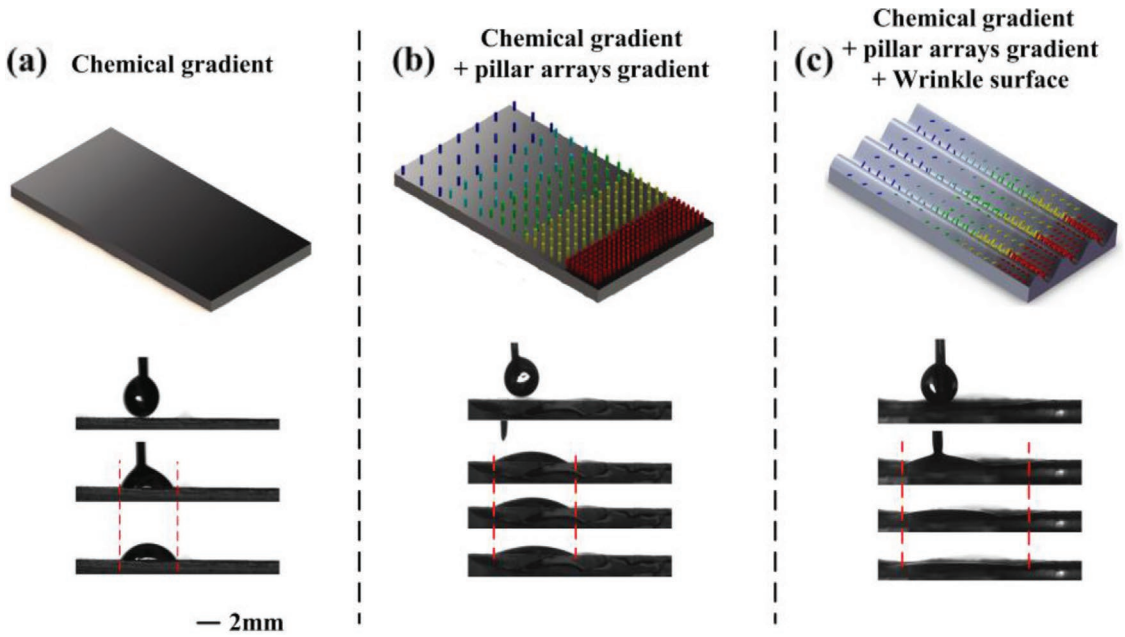

Figure 4. Droplet movement behavior on the surfaces with a) chemical gradient, b) chemical gradient and pillar arrays gradient, c) double-gradient wrinkled structure. The scale bar is 2 mm.

2.5. In Situ Regulation of External Strain and Its Effect to the Spreading Length of Droplets

We also studied in situ regulation of external strain and its effect to the spreading length of droplets on the double-gradient wrinkled surface. The in situ regulation process is schematically shown in **Figure 7**a. A 200% external tensile strain was applied to a wrinkled surface with ε_{pre} = 200%; then, a 5 µL droplet was placed onto the surface. After the applied external tensile strain was completely released (residual strain ε_{res} = 0%), the droplet spreads a length of 10.5 mm along the axial direction of the wrinkled structure. This state was defined as the original state. Next, we slowly stretched the double-gradient wrinkled surface and found that the droplet spreading length along the axial direction of the wrinkled structure decreased, and meanwhile, the droplet spread shorter distance along the direction perpendicular to the wrinkled structure. The reason is that when the strain is applied, the wrinkle structure size (A/λ) decreases, the droplets more easily overcome the energy barrier in the direction perpendicular to the axial direction of the wrinkle structure. This first cycle process is shown in Figure 7b, and the spreading length of the droplet changes from 10.5 to 6.8 mm with the anisotropy index changing from 6.25 to 2. Optical images of the droplet spreading and the physical stretching device are shown in Figure S10, Supporting Information. By repeating this process, we find that the spreading length of the droplet fluctuates between 10.5 ± 0.5 mm and 6.8 ± 0.6 mm during 50 cycles, showing good repeatability and mechanical stability (Figure 7c).

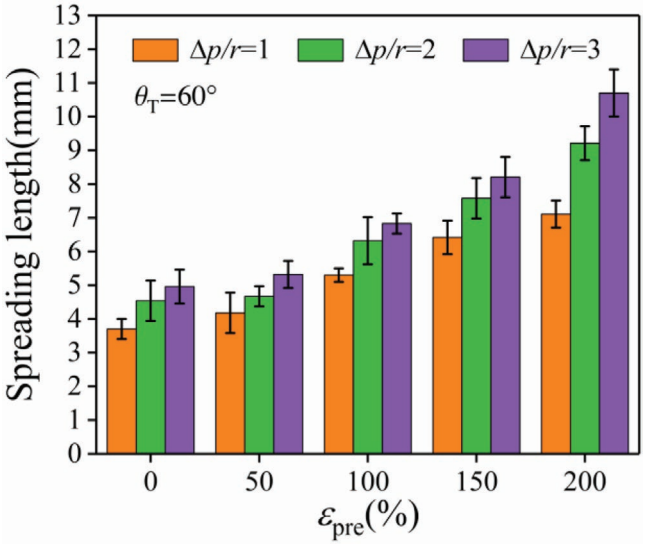

Figure 5. Experimental data for the spreading length of the droplets on double-gradient wrinkled surface under different pre-strain ε_{pre} values. The pillar arrays shown here are the pillar arrays with $\Delta p/r = 1$, $\Delta p/r = 2$, and $\Delta p/r = 3$. The chemical gradient shown here is $\theta_T = 60°$. ε_{pre} = 0%, 50%, 100%, 150%, and 200%.

Figure 8a shows the difference in the spreading/transport length of a droplet under different external stimuli. Compared to other external stimuli which in situ regulate the spreading or moving length of the droplets, the double-gradient wrinkled surface adjusted under mechanical strain allows the droplet to be spread to a moderate distance directionally and can reversibly fluctuate the spreading length and anisotropy within a wide range under external strain stimulation (Figure 8). Our work may provide a new method for the in situ regulation of the directional spreading of droplets on a flexible substrate.

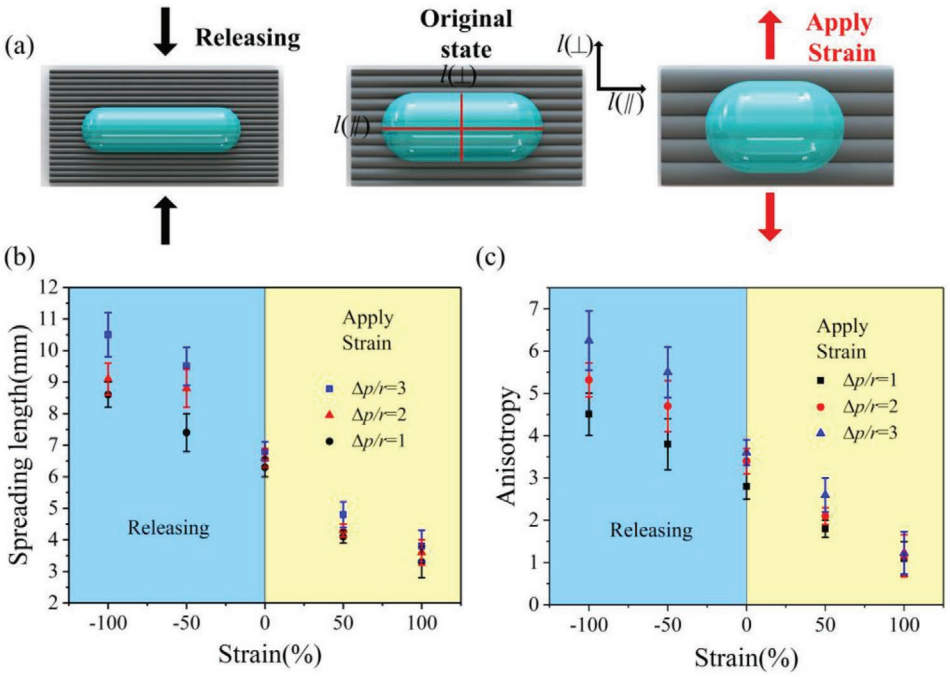

Figure 6. Ex situ external strain regulation to the spreading length of a droplet. a) Schematic diagram of ex situ external strain regulation. b) Experimental data show the spreading length under external strain. The droplet can spread further during the releasing process, but spreads a shorter distance during the stretching process. c) Experimental data of the anisotropy under external strain.

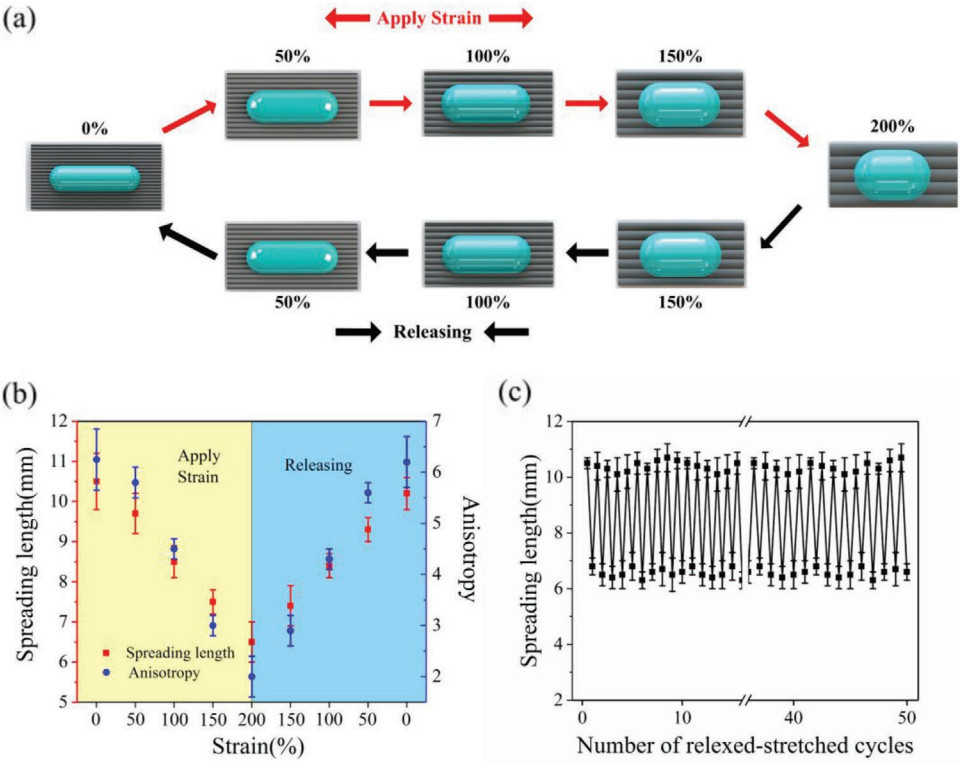

Figure 7. In situ external strain regulation and its effect to the spreading length of the droplet. a) Schematic diagram of in situ external strain regulation. The structure is first pre-stretched to 200%, then a 5 µL droplet is placed onto the surface. After that, the structure is slowly released, stretched, and rereleased. b) Changes in droplet length and anisotropy during the first cycle of stretching and relaxation. c) Repeated stretching and relaxation shows good repeatability and mechanical stability.

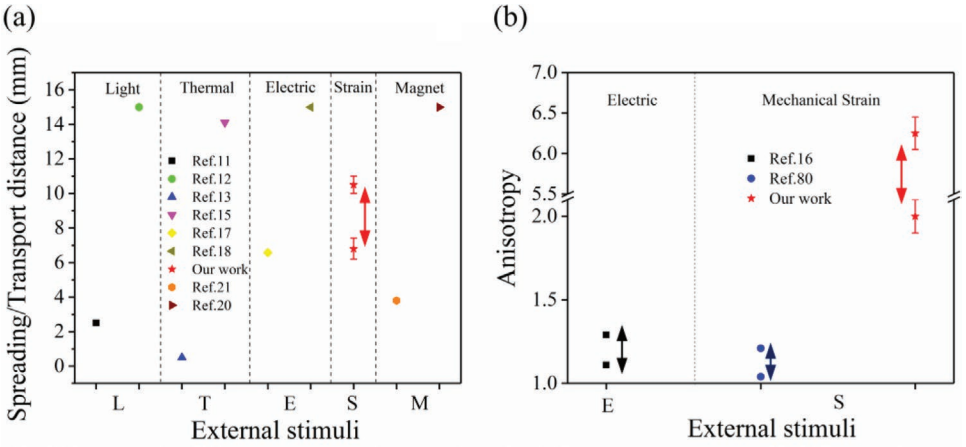

Figure 8. In situ adjustment of surface wettability under different stimulation methods. a) Spreading/transport length of a droplet under different external stimuli. b) Anisotropy of droplets with different external stimuli on an anisotropic surface. The two-way arrows represent reversible transitions.

3. Conclusion

A double-gradient wrinkled surface that enables droplets to spread over a larger distance and the spreading length of droplets to be regulated in situ by applying external strain has been proposed. Specifically, we studied the wetting behavior of surfaces with pillar arrays gradients, chemical gradients and composite gradients. We find that droplets can spread over a larger distance on a surface with $\Delta p/r = 3$ and $\theta_T = 60°$. Next, we explored the effect of the wrinkle structure on the wetting behavior of surfaces with composite gradient. Experimentally, we find that the wrinkle structure that is formed by 200% pre-stretching provides the most obvious optimization for the spreading length of a 5 µL droplet, which can reach 10.7 mm on the double-gradient wrinkled surface ($\Delta p/r = 3$, $\theta_T = 60°$, $\varepsilon_{pre} = 200\%$). Finally, in situ and ex situ regulation of the droplet spreading length was realized by applying external strain. The spreading length of a 5 µL droplet fluctuates between 10.5 ± 0.5 and 6.8 ± 0.6 mm under the effect of external strain. Our work may provide a new method for the regulation of the directional spreading of droplets on a soft surface. This dynamically tunable wettability has great promise for use in flexible electronics, microfluidics, and drug delivery.

4. Experimental Section

Fabrication of the Double-Gradient Wrinkled Structure: The route for the fabrication of the double-gradient wrinkled structure was schematically shown in Figure S1, Supporting Information. The polydimethylsiloxane (PDMS, Sylgard 184, Dow Corning) pre-polymer and the cross-linker were mixed at a mass ratio of 10:1, and then the mixture was placed in a vacuum atmosphere for 20 min to remove bubbles after stirring. Subsequently, a PDMS layer (elastic modulus of 2 Mpa, thickness of 150 µm) was obtained by spin-coating treated PDMS mixture (with a rotate speed of 8000 rpm) on a hydrophobic-treated silicon template by using *N*-heptane, ethyl acetate, and trimethoxyoctadecylsilane (corresponding volume ratio of 1000:50:20, Figure S1a, Supporting Information). The commercial silicon template with gradient hole arrays was fabricated by a micromachining technology. Then the sample was placed on a baking table and cured at 80 °C for 5 min to form partially cross-linked PDMS. After that, the very high bonding tapes (VHB tapes, elastic modulus of 0.04 Mpa, thickness of 1 mm) was stretched to a certain length (Figure S1b, Supporting Information) and the PDMS layer was transferred to the pre-stretched VHB tapes surface. The assembly was baked at 80 °C for 3 h to cure the PDMS layer (Figure S1c, Supporting Information). After the silicon template was peeled off, and the pre-stretched VHB tapes was released (Figure S1d,e, Supporting Information), a wrinkled structure with gradient micro-pillar arrays was eventually obtained. The pillar arrays had the given radius ($r = 5$ µm) and adjustable center distance between two adjacent pillars ($p = 20$, 35, 50, 65 and 80 µm).

To create a chemical gradient on the wrinkled structure with gradient micro-pillar arrays, the sample was placed on a slide glass with a thin metal shield at a "wedge" angle (Figure S1f, Supporting Information) and treated in a plasma generator for 20 s (Figure S1g, Supporting Information). In order to maintain the plasma-treated chemical gradient in the air atmosphere for a prolonged time, the sample was soaked in Poly dimethyl diallyl ammonium chloride (PDDA) solution for 20 min for maintaining the wettability of PDMS surface after plasma treatment and then washed excess PDDA solution with deionized water and placed in a blast oven at 70 °C for 30 min for drying. Finally, the double-gradient wrinkled structure was obtained.

Surface Topography and Droplet Spreading Measurements: The morphology of the surface was analysed by scanning electron microscopy (SEM, Hitachi S4800) and the laser microscope (Keyence, VK-X110). The droplet contact angle (CA, θ) was measured using 4 µL droplets of deionized water with a contact angle instrument (Thermo, DCA-322). The water drops were dispensed using a syringe pump through a needle with 100 µm inner diameter. Images of the spreading of the droplet on the samples were captured by a CCD camera equipped with a magnifying lens at the ambient temperature.

Supporting Information

Supporting Information is available from the Wiley Online Library or from the author.

Acknowledgements

This work was supported by the National Natural Science Foundation of China (grant nos. 11672269, 11972323, 51572242, and 51675485), the Zhejiang Provincial Natural Science Foundation of China (grant nos. LR20A020002, LR19E020004, and LR18E050002) and the Fundamental Research Funds for the Provincial Universities of Zhejiang (RF-B2019004).

Conflict of Interest

The authors declare no conflict of interest.

Keywords

gradient surfaces, mechanical regulation, surface wetting, unidirectional spreading

Received: November 25, 2019
Revised: January 22, 2020
Published online:

[1] B. Chang, A. Shah, I. Routa, H. Lipsanen, Q. Zhou, *Appl. Phys. Lett.* **2012**, *101*, 114105.
[2] H. W. Chen, L. W. Zhang, D. Y. Zhang, P. F. Zhang, Z. W. Han, *ACS Appl. Mater. Interfaces* **2015**, *7*, 13987.
[3] S. Daniel, M. K. Chaudhury, J. C. Chen, *Science* **2001**, *291*, 633.
[4] Y. S. Yu, M. C. Wang, X. Huang, *Sci. Rep.* **2017**, *7*, 14118.
[5] J. Zhang, C. Zhu, J. Lv, W. Zhang, J. Feng, *ACS Appl. Mater. Interfaces* **2018**, *10*, 40219.
[6] I. E. Agranovski, R. D. Braddock, *AIChE J.* **1998**, *44*, 2775.
[7] V. Srinivasan, V. K. Pamula, R. B. Fair, *Lab Chip* **2004**, *4*, 310.
[8] X. H. Wang, A. P. Liu, Y. Xing, H. W. Duan, W. Z. Xu, Q. Zhou, H. P. Wu, C. Chen, B. Y. Chen, *Biosens. Bioelectron.* **2018**, *105*, 22.
[9] S. Li, J. Liu, J. Hou, *Sci. Rep.* **2016**, *6*, 37888.
[10] X. Bai, Y. Shen, H. Tian, Y. Yang, H. Feng, J. Li, *Sep. Purif. Technol.* **2019**, *210*, 402.
[11] K. Ichimura, S. K. Oh, M. Nakagawa, *Science* **2000***288*, 1624.
[12] J. A. Lv, Y. Liu, J. Wei, E. Chen, L. Qin, Y. Yu, *Nature* **2016**, *537*, 179.
[13] P. H. Xue, J. J. Nan, T. Q. Wang, S. Wang, S. S. Ye, J. H. Zhang, Z. C. Cui, B. Yang, *Small* **2017**, *13*, 1601807.
[14] L. L. Wang, L. P. Heng, L. Jiang, *ACS Appl. Mater. Interfaces* **2018**, *10*, 7442.
[15] C. L. Gao, L. Wang, Y. C. Lin, J. T. Li, Y. F. Liu, X, Li , S. L. Feng, Y. M. Zheng, *Adv. Funct. Mater.* **2018**, *28*, 1803072.
[16] V. Parihar, S. Bandyopadhyay, S. Das, S. Dasgupta, *Langmuir* **2018**, *34*, 1844.
[17] T. Yasuda, K. Imamura, K. Hirase, in *TRANSDUCERS 2009–2009 Int. Solid-State Sensors, Actuators and Microsystems Conf.*, IEEE, Piscataway, NJ **2009**, pp. 413–416.
[18] D. L. Tian, L. L. He, N. Zhang, X. Zheng, Y. H. Dou, X. F. Zhang, Z. Y. Guo, L. Jiang, *Adv. Funct. Mater.* **2016**, *26*, 7986.
[19] P. D. Che, L. P. Heng, L. Jiang, *Adv. Funct. Mater.* **2017**, *27*, 1606199.
[20] D. L. Tian, N. Zhang, X. Zheng, G. L. Hou, Y. Tian, Y. Du, L. Jiang, S. X. Dou, *ACS Nano* **2016**, *10*, 6220.
[21] Y. C. Lin, Z. Y. Hu, M. X. Zhang, T. Xu, S. L. Feng, L. Jiang, Y. M. Zheng, *Adv. Funct. Mater.* **2018**, *28*, 1800163.
[22] S. G. Lee, D. Y. Lee, H. S. Lim, D. H. Lee, S. Lee, K. Cho, *Adv. Mater.* **2010**, *22*, 5013.
[23] G. J. Lin, P. Chandrasekaran, C. J. Lv, Q. T. Zhang, Y. C. Tang, L. Han, J. Yin, *ACS Appl. Mater. Interfaces* **2017**, *9*, 26510.
[24] B. E. Pinchasik, H. Q. Wang, H. Möhwald, H. Asanuma, *Adv. Mater. Interfaces* **2016**, *3*, 1600722.
[25] P. Goel, S. Kumar, J. Sarkar, J. P. Singh, *ACS Appl. Mater. Interfaces* **2015**, *7*, 8419.
[26] H. P. Wu, S. H. Yu, Z. X. Xu, B. B. Cao, X. Peng, Z. Zhang, G. Z. Chai, A. P. Liu, *Langmuir* **2019**, *35*, 6870.
[27] N. Wang, D. Xiong, Y. Deng, Y. Shi, K. Wang, *ACS Appl. Mater. Interfaces* **2015**, *7*, 6260.
[28] D. Bonn, J. Eggers, J. Indekeu, J. Meunier, E. Rolley, *Rev. Mod. Phys.* **2009**, *81*, 739.
[29] A. Marmur, *Langmuir* **2003**, *19*, 8343.
[30] D. Quéré, *Annu. Rev. Mater. Res.* **2008**, *38*, 71.
[31] N. L. Abbott, J. P. Folkers, G. M. Whitesides, *Science* **1992**, *257*, 1380.
[32] H. P. Wu, K. Zhu, B. B. Wu, J. Lou, Z. Zhang, G. Z. Chai, *Appl. Surf. Sci.* **2016**, *382*, 111.
[33] T. Onda, S. Shibuichi, N. Satoh, K. Tsujii, *Langmuir* **1996**, *12*, 2125.
[34] H. P. Wu, Z. Yang, B. B. Cao, Z. Zhang, K. Zhu, B. B. Wu, S. F. Jiang, G. Z. Chai, *Langmuir* **2017**, *33*, 407.
[35] H. P. Wu, K. P. Jiang, Z. X. Xu, S. H. Yu, X. Peng, Z. Zhang, H. Bai, G. Z. Chai, *Langmuir* **2019**, *35*, 17000.
[36] X. G. Qiu, Z. Yang, H. P. Wu, J. Guo, Z. Zhang, J. Feng, A. P. Liu, *Appl. Surf. Sci.* **2018**, *456*, 602.
[37] H. P. Wu, K. Zhu, B. B. Cao, Z. Zhang, B. B. Wu, L. H. Liang, A. P. Liu, *Soft Matter* **2017**, *13*, 2995.
[38] S. L. Feng, S. J. Wang, L. C. Gao, G. J. Li, Y. P. Hou, Y. M. Zheng, *Angew. Chem., Int. Ed.* **2014**, *53*, 6163.
[39] S. C. Hernandez, C. J. C. Bennett, C. E. Junkermeier, S. D. Tsoi, F. J. Bezares, R. Stine, J. T. Robinson, E. H. Lock, D. R. Boris, B. D. Pate, J. D. Caldwell, T. L. Reinecke, P. E. Sheehan, S. G. Walton, *ACS Nano* **2013**, *7*, 4746.
[40] S. Y. Deng, W. F. Shang, S. L. Feng, S. P. Zhu, Y. Xing, D. Li, Y. P. Hou, Y. M. Zheng, *Sci. Rep.* **2017**, *7*, 45687.
[41] P. Ge, S. L. Wang, W. D. Liu, T. Q. Wang, N. Z. Yu, P. H. Xue, H. X. Chen, H. Z. Shen, J. H. Zhang, B. Yang, *Adv. Mater. Interfaces* **2017**, *4*, 1700034.
[42] M. Wang, Q. Liu, H. R. Zhang, C. Wang, L. Wang, B. X. Xiang, H. T. Fang, C. F. Guo, S. C. Ruan, *ACS Appl. Mater. Interfaces* **2017**, *9*, 29248.
[43] M. Gürsoy, M. T. Harris, A. Carletto, A. E. Yaprak, M. Karaman, J. P. S. Badyal, *Colloids Surf. A* **2017**, *529*, 959.
[44] K. H. Chu, R. Xiao, E. N. Wang, *Nat. Mater.* **2010**, *9*, 413.
[45] H. W. Chen, L. W. Zhang, P. F. Zhang, D. Y. Zhang, Z. W. Han, L. Jiang, *Small* **2017**, *13*, 1601676.
[46] P. F. Zhang, H. W. Chen, L. Li, H. L. Liu, G. Liu, L. W. Zhang, D. Y. Zhang, L. Jiang, *ACS Appl. Mater. Interfaces* **2017**, *9*, 5645.
[47] H. W. Chen, P. F. Zhang, L. W. Zhang, H. L. Liu, Y. Jiang, D. Y. Zhang, Z. W. Han, L. Jiang, *Nature* **2016**, *532*, 85.
[48] J. Li, X. Zhou, J. Li, L. Che, J. Yao, G. McHale, M. Chaudhury, Z. Wang, *Sci. Adv.* **2017**, *3*, eaao3530.
[49] C. X. Li, N. Li, X. S. Zhang, Z. C. Dong, H. W. Chen, L. Jiang, *Angew. Chem., Int. Ed.* **2016**, *55*, 14988.
[50] M. Y. Cao, X. Jin, Y. Peng, C. M. Yu, K. Li, K. S. Liu, L. Jiang, *Adv. Mater.* **2017**, *29*, 1606869.
[51] W. Z. Xu, Y. Xing, J. Liu, H. P. Wu, Y. Cui, D. W. Li, D. Y. Guo, C. R. Li, A. P. Liu, H. Bai, *ACS Nano* **2019**, *13*, 7930.
[52] J. T. Yang, J. C. Chen, K. J. Huang, J. A. Yeh, *J. Microelectromech. Syst.* **2006**, *15*, 697.
[53] Y. Zhang, X. J. Wang, S. H. Ma, K. P. Jiang, X. J. Han, *RSC Adv.* **2016**, *6*, 11325.
[54] Y. H. Lai, J. T. Yang, D. B. Shieh, *Lab Chip* **2010**, *10*, 499.
[55] J. Zhang, Y. Han, *Langmuir* **2008**, *24*, 796.
[56] D. Y. Xia, L. M. Johnson, G. P. López, *Adv. Mater.* **2012**, *24*, 1287.
[57] M. X. Zhang, L. Wang, Y. P. Hou, W. W. Shi, S. L. Feng, Y. M. Zheng, *Adv. Mater.* **2015**, *27*, 5057.
[58] J. N. Wang, Y. Q. Liu, Y. L. Zhang, J. Feng, H. Wang, Y. H. Yu, H. B. Sun, *Adv. Funct. Mater.* **2018**, *28*, 1800625.
[59] J. Y. Long, P. X. Fan, D. F. Jiang, J. P. Han, Y. Lin, M. Y. Cai, H. J. Zhang, M. L. Zhong, *Adv. Mater. Interfaces* **2016**, *3*, 1600641.
[60] P. C. Zhang, H. L. Liu, J. X. Meng, G. Yang, X. L. Liu, S. T. Wang, L. Jiang, *Adv. Mater.* **2014**, *26*, 3131.
[61] Z. Q. Zhang, T. Zhang, Y. W. Zhang, K. S. Kim, H. J. Gao, *Langmuir* **2012**, *28*, 2753.
[62] A. Takei, M. Murano, M. Tani, H. Fujita, K. Okumura, *Appl. Phys. Lett.* **2017**, *110*, 161602.

[63] S. Schauer, M. Worgull, H. Hölscher, *Soft Matter* **2017**, *13*, 4328.
[64] R. Prathapan, J. D. Berry, A. Fery, G. Garnier, R. F. Tabor, *ACS Appl. Mater. Interfaces* **2017**, *9*, 15202.
[65] P. K. Roy, R. Pant, A. K. Nagarajan, K. Khare, *Langmuir* **2016**, *32*, 5738.
[66] S. K. Saha, M. L. Culpepper, *Langmuir* **2016**, *18*, 938.
[67] J. L. Liu, X. Q. Feng, G. F. Wang, S. W. Yu, *J. Phys.: Condens. Matter* **2007**, *19*, 356002.
[68] L. Tie, Z. G. Guo, Y. M. Liang, W. M. Liu, *Nanoscale* **2019**, *11*, 3725.
[69] D. Qin, Y. N. Xia, G. M. Whitesides, *Nat. Protoc.* **2010**, *5*, 491.
[70] F. Barkusky, C. Peth, A. Bayer, K. Mann, *J. Appl. Phys.* **2007**, *101*, 124908.
[71] A. M. Coclite, R. M. Howden, D. C. Borrelli, C. D. Petruczok, R. Yang, J. L. Yague, A. Ugur, N. Chen, S. H. Lee, W. J. Jo, *Adv. Mater.* **2013**, *25*, 5392.
[72] W. R. Childs, M. J. Motala, K. J. Lee, R. G. Nuzzo, *Langmuir* **2005**, *21*, 10096.
[73] P. Goel, S. Kumar, R. Kapoor, J. P. Singh, *Appl. Surf. Sci.* **2015**, *356*, 102.
[74] J. Y. Chung, J. P. Youngblood, C. M. Stafford, *Soft Matter* **2007**, *3*, 1163.
[75] S. Yang, K. Khare, P. C. Lin, *Adv. Funct. Mater.* **2010**, *20*, 2550.
[76] S. Zhao, H. Xia, D. Wu, C. Lv, Q. D. Chen, K. Ariga, L. Q. Liu, H. B. Sun, *Soft Matter* **2013**, *9*, 4236.
[77] L. Tie, J. Li, Z. Guo, Y. Liang, W. Liu, *Colloids Surf. A* **2019**, *562*, 170.
[78] X. Liu, C. Hong, Y. Ding, X. Liu, J. Yao, S. Dai, *Chin. Phys. B* **2019**, *28*, 014703.
[79] D. Rhee, W. K. Lee, T. W. Odom, *Angew. Chem., Int. Ed.* **2017**, *56*, 6523.
[80] D. Kwon, S. Wooh, H. Yoon, K. Char, *Langmuir* **2018**, *34*, 4732.
[81] J. H. Lee, H. W. Ro, R. Huang, P. Lemaillet, T. A. Germer, C. L. Soles, C. M. Stafford, *Nano Lett.* **2012**, *12*, 5995.
[82] P. C. Lin, S. Yang, *Soft Matter* **2009**, *5*, 1011.
[83] F. Mumm, A. T. J. van Helvoort, P. Sikorski, *ACS Nano* **2009**, *3*, 2647.
[84] J. Y. Chung, A. J. Nolte, C. M. Stafford, *Adv. Mater.* **2011**, *23*, 349.
[85] Z. Y. Huang, W. Hong, Z. Suo, *J. Mech. Phys. Solids* **2005**, *53*, 2101.
[86] M. K. Chaudhury, G. M. Whitesides, *Science* **1992**, *256*, 1539.
[87] S. Daniel, M. K. Chaudhury, *Langmuir* **2002**, *18*, 3404.
[88] O. Bliznyuk, H. P. Jansen, E. S. Kooij, H. J. Zandvliet, B. Poelsema, *Langmuir* **2011**, *27*, 11238.

